

Comparative proteome analysis of retinal hypoxia–ischemia in acute ocular hypertension model with TMT-based quantitative proteomics

Guangyi Huang¹, Yunru Lin¹, Fen Tang¹, Hui Huang¹, Qi Chen¹, Ning Su¹, Ling Cui¹, Fan Xu¹, and Chaolan Shen¹

¹People’s Hospital of Guangxi Zhuang Autonomous Region

March 07, 2024

Abstract

Acute glaucoma’s main sign is acute ocular hypertension (AOH), leading to retinal ganglion cell (RGC) death and irreversible visual loss. However, there is currently no approved effective therapy for this condition. This research aimed to identify the major regulators and the overall protein changes involved in AOH-induced RGC death. Mass-spectrometry was used to analyze proteomic patterns in the retinal protein extracts from the AOH and sham-group, and then Gene Ontology (GO) and Kyoto Encyclopedia of Genes and Genomes (KEGG) pathway studies were performed. In proteomics analysis, we identified 92 proteins in the AOH group compared to the control group, with 58 proteins being up-regulated and 34 proteins being down-regulated. Western blot and biochemical assay analyses identified changes in Fatty acid-binding protein 7 (FABP7), and caveolin-1 (Cav-1) that were related to fatty acid metabolism and ocular inflammatory signaling. Moreover, variations in the expression of the proteins Galectin-1 (Gal-1), S100 calcium-binding protein A6 (S100a6), and Visinin-like protein-1 (VILIP) was shown, all of which were associated to the process of neuronal ischemia. Our investigation demonstrated that neuroinflammation and fatty acid metabolism were involved in retinal impairment following AOH, offering a potential therapeutic strategy for acute glaucoma.

Comparative proteome analysis of retinal hypoxia–ischemia in acute ocular hypertension model with TMT-based quantitative proteomics

Guangyi Huang^{1,2} #; Yunru Lin^{1,3} #; Fen Tang¹; Hui Huang¹; Qi Chen¹; Ning Su¹; Ling Cui¹; Fan Xu¹; Chaolan Shen¹ *

¹Department of Ophthalmology, the People’s Hospital of Guangxi Zhuang Autonomous Region & Guangxi Key Laboratory of Eye Health & Guangxi Health Commission Key Laboratory of Ophthalmology and Related Systemic Diseases Artificial Intelligence Screening Technology & Institute of Ophthalmic Diseases, Guangxi Academy of Medical Sciences, Nanning 530021, China

2 Guilin Medical University, Guilin 541000, China

3 Youjiang Medical University for Nationalities, Baise 533000, China

* Corresponding author: Chaolan Shen, Tel.:0086-0771-2186320, E-mail: shenchaolaneye@163.com, Department of Ophthalmology, the People’s Hospital of Guangxi Zhuang Autonomous Region, No. 6 Taoyuan Road, Qingxiu District, Nanning 530021, PR China

These authors contributed equally to this work.

Abstract

Acute glaucoma's main sign is acute ocular hypertension (AOH), leading to retinal ganglion cell (RGC) death and irreversible visual loss. However, there is currently no approved effective therapy for this condition. This research aimed to identify the major regulators and the overall protein changes involved in AOH-induced RGC death. Mass-spectrometry was used to analyze proteomic patterns in the retinal protein extracts from the AOH and sham-group, and then Gene Ontology (GO) and Kyoto Encyclopedia of Genes and Genomes (KEGG) pathway studies were performed.

In proteomics analysis, we identified 92 proteins in the AOH group compared to the control group, with 58 proteins being up-regulated and 34 proteins being down-regulated. Western blot and biochemical assay analyses identified changes in Fatty acid-binding protein 7 (FABP7), and caveolin-1(Cav-1) that were related to fatty acid metabolism and ocular inflammatory signaling. Moreover, variations in the expression of the proteins Galectin-1 (Gal-1), S100 calcium-binding protein A6 (S100a6), and Visinin-like protein-1 (VILIP) was shown, all of which were associated to the process of neuronal ischemia. Our investigation demonstrated that neuroinflammation and fatty acid metabolism were involved in retinal impairment following AOH, offering a potential therapeutic strategy for acute glaucoma.

Significance: Ischemia-reperfusion (I/R) retinal disorders play a significant role in acute glaucoma. Pathological cell death in the retina due to I/R injury may involve fatty acid metabolism and ocular inflammation. This study suggests that AOH-induced retinal neuronal cell death might be influenced by the interaction between FABP7 and Caveolin-1 in the PPAR/JAK-STAT signaling pathway. Neuroinflammation and fatty acid metabolism appear to be critical factors in retinal impairment following AOH, offering promising therapeutic targets for acute glaucoma.

Keywords: Acute glaucoma, Proteomics, Retina, Neurodegeneration, FABP7, Caveolin-1

Abbreviations:

AOH: acute ocular hypertension

Cav-1: caveolin-1

DHA: docosahexaenoic acid

FABP7: Fatty acid-binding protein 7

GO: Gene Ontology

Gal-1: Galectin-1

IOP: intraocular pressure

KEGG: Kyoto Encyclopedia of Genes and Genomes

OGDR: glucose deprivation/reoxygenation

PUFAs: polyunsaturated fatty acids

RGC: retinal ganglion cell

RIR: retinal ischemia/ reperfusion

S100a6: S100 calcium-binding protein A6

TMT: Tandem mass tag

VILIP: Visinin-like protein-1

Introduction

Glaucoma, a major cause of vision impairment, is expected to cause blindness in around 111.8 million individuals worldwide by 2040[1]. Acute glaucoma, which is more prevalent among Asians and East Indians, is a subtype of primary angle-closure glaucoma[2]. In acute glaucoma, the intraocular pressure (IOP) increases

at a faster pace than the retinal perfusion pressure, which could lead to retinal ischemia/ reperfusion (RIR) injury, optic nerve damage, and death of RGCs. However, the intricate pathophysiology of IOP-induced optic nerve injury is still not fully elucidated. The current recommended treatment for glaucoma is persistent IOP reduction, which can slow but not halt the disease's progression[3,4].

The analysis of protein changes plays a critical role in the analytical tools used to comprehend the mechanisms of pathogenesis underlying glaucomatous neurodegeneration. Multiplexing high-throughput protein profiling is an invaluable aid in this area, facilitating a better understanding of this intricate neurodegenerative disease and the development of treatments for it. Therefore, glaucoma researchers frequently investigate protein expression, modifications, and protein-protein interactions in experimental models and postmortem human tissues from individuals with glaucoma, alongside the expanding use of genetic and transcriptome analysis[5-9].

Tandem mass tag (TMT) labeling coupled with liquid chromatography-tandem mass spectrometry (LC-MS/MS) has emerged as the preferred method for protein quantitation. The utilization of TMT labeling in conjunction with LC-MS/MS offers several distinct advantages over the outdated 2D-DIGE method. This innovative technique provides enhanced accuracy and reliability in quantitative data analysis, enabling the identification of proteins with a broader range of molecular weights and abundance levels. Moreover, this advanced method is applicable to a wide array of samples, including cellular extracts and complex mixtures, and demonstrates superior sensitivity, specificity, accuracy, and reproducibility in its analyses.

Considering the complexity of glaucoma and the limitations associated with human samples, it is essential to establish an animal model that directly replicates the pathogenesis of human acute glaucoma. The mouse acute ocular hypertension model is a commonly used animal model that can mimic the typical alterations in retinal hypoxia-ischemia phenotypes seen in acute glaucoma [10,11]. In this study, the proteome of retinal tissue from an AOH model was examined using a TMT-based quantitative proteomic approach and compared to a control group to understand the biochemical changes that occur during the evolution of acute glaucoma and to identify potential biomarkers. Our results identified DEPs in the retina of AOH mice, which were involved in the dysregulation of specific metabolic pathways significantly. In particular, FABP7 and Cav-1 were significantly up-regulated in injured retinas. Therefore, we propose that FABP7 and Cav-1 may serve as potential targets for treating acute glaucoma.

2 Material and methods

2.1 Animal model of retinal ischemic injure and grouping

For this study, we selected male C57BL/6J mice aged between 6 to 8 weeks (20–25 g), and purchased from the Guangxi Medical University. The mice were maintained in a 12-h light/dark cycle (lights on from 8:00 a.m. to 8:00 p.m.) with food and water ad libitum. The study protocols had the approval by ethical committee of The People's Hospital of Guangxi Zhuang Autonomous Region (No. KY-GZR-2019-053). All animal cares and experimentations were carried out based on the Association for Research in Vision and Ophthalmology Statement for the Use of Animals in Ophthalmic and Vision Research.

To induce AOH injury in the mice, a precise and careful protocol was followed.[12] The mice were first anesthetized with a 1% pentobarbital solution. To further minimize any discomfort, a topical anesthetic of 0.5% tetracaine hydrochloride was applied to the cornea, and 0.5% tropicamide phenylephrine eye drops were used to dilate the pupil. Using a 32-gauge sterile needle, the anterior chamber of the right eye was perfused with sterilized normal saline, which was connected to a reservoir in the nasal direction. The intraocular pressure was then raised and maintained at 110 mmHg by elevating the reservoir to a height of 150 cm. This ensured that the AOH injury was induced and sustained over a period of one hour. Intraocular pressure was raised to 110 mmHg for 60 minutes; the needle was then removed to allow natural retinal reperfusion[12,13].After this time, the needle was gently withdrawn. The left eye, which was cannulated without elevating the reservoir, served as the control eye or the sham group.

2.2 Protein Extraction and Trypsin Digestion and LC-MS/MS

In this study, retinal tissues from five AOH and Sham mice were combined into a single tube to create pooled samples for proteomics analyses. Three replicates of pooled samples were used for each group, resulting in a total of 15 retinas per group. The samples were flash-frozen in liquid nitrogen and stored at -80°C until use. To extract the proteins, the retinal sample was added to Sodium Dodecyl sulfate and Tris buffer (SDT) buffer and then sonicated and boiled for 10 minutes. After centrifugation at 14,000 xg for 15 minutes at 4°C , the supernatant was collected and the protein concentration was determined using the BCA Protein Assay Kit (Beyotime). Any remaining debris was removed during the centrifugation step.

The digestion process for the samples involved reducing 150-200 μg of proteins with DL-dithiothreitol (Sigma, USA) at 100°C for 5 minutes. The resulting mixture was then purified using UA buffer (8 M Urea, 150 mM Tris-HCl pH 8.5) through multiple rounds of ultrafiltration (Sartorius, 30 kD) to remove unwanted low-molecular-weight components. To block reduced cysteine residues, 100 μl of iodoacetamide (100 mM IAA in UA buffer) was added to the samples, which were then incubated in darkness for 30 minutes. After washing the filters three times with 100 μl of UA buffer, followed by two washes with 100 μl of 0.1M TEAB buffer, the protein suspensions were digested overnight at 37°C with 4 μg trypsin (Promega) in 40 μl 0.1M TEAB buffer. The peptide content was estimated by measuring the UV light spectral density at 280 nm, using an extinction coefficient of 1.1 of 0.1% (g/l) solution, which was calculated based on the frequency of tryptophan and tyrosine in vertebrate proteins. We used the TMT 10-plex system (Thermo Fisher Scientific) for TMT-labeling, 100 μg of each sample was used with TMT reagent.

LC-MS/MS analysis was conducted using a Q Exactive PLUS mass spectrometer (Thermo Fisher Scientific) that was coupled to an Easy nLC system (Thermo Fisher Scientific) for 90 minute. The mass spectrometer was operated in positive ion mode, and survey scans were acquired at a resolution of 70000 at m/z 200 with an AGC target of $3e6$ and a maxIT of 50 ms. MS2 scans were acquired at a resolution of either 17500 or 35000 for HCD spectra at m/z 200 with an AGC target of $2e5$ and a maxIT of 50 ms, and the isolation width was set to 2.0 m/z . Only ions with a charge state between 2-6 and a minimum intensity of $2e3$ were selected for fragmentation, and dynamic exclusion for selected ions was set to 30 seconds. The normalized collision energy was set to 30 eV.

2.3 Data Analysis

The MS/MS raw files were processed using the MASCOT engine (Matrix Science, London, UK; version 2.6) integrated into Proteome Discoverer 2.2 and searched against the database (Uniprot_MusMusculus_17082.-20210928_swissprot). The search parameters included trypsin as the enzyme used to generate peptides, with a maximum of 2 missed cleavages permitted. A precursor mass tolerance of 10 ppm was specified, along with a 0.05 Da tolerance for MS2 fragments. Carbamidomethyl (C) was set as a fixed modification, while variable modifications included Oxidation (M) and Acetyl (Protein N-term), except for TMT labels. A peptide and protein false discovery rate of 1% was enforced using a reverse database search strategy.

Data Availability

The MS proteomics data have been deposited to the PRIDE Archive (<http://www.ebi.ac.uk/pride/archive/>) via the PRIDE partner repository with the data set identifier PXD042988.

2.4 Bioinformatics Analysis

The identified differentially abundance proteins were analyzed using GO terms (database version: go.-201504.obo) of the sequence with the top Bit-Score by Blast2GO. The annotation from GO terms to proteins was completed by Blast2GO Command Line. After the elementary annotation, InterProScan was used to search the EBI database by motif, and the functional information of the motif was added to proteins to improve annotation. ANNEX was used to further improve the annotation and connection between GO terms. Pathway analysis was performed using the KEGG database, and protein clusters with a False discovery rate < 0.05 , and correlation value $[?]$ 0.7 were considered statistically significant compared to the original ertapenem untreated time point.

2.5 Verification of Candidate Proteins by qRT-PCR

The decidual immune cells were subjected to RNA extraction using TRIzol reagent (Takara Biotechnology, Inc., Japan) following the manufacturer’s protocol. Primers were designed by Takara Biotechnology and the sequences were blasted (Table 1). The resulting cDNA was synthesized using the PrimeScript RT-PCR Kit (Takara) and amplified with duplicate SYBR Green real-time PCR reagent (Roche). The β -actin gene was used as an endogenous control to normalize the data.

Table 1 List primers of identified proteins by real-time PCR

FABP7	forward: TGAAACCACTGCAGATGATAGAA
	reverse: TTTCTTTGCCATCCCATTTC
Caveolin1	forward: CACACCAAGGAGATTGACCTGG
	reverse: CCTTCCAGATGCCGTCGAAACT
S100a6	forward: TACTCTGGCAAGGAAGGT
	reverse: CAGGAAGGCGACATACTC
Galectin	forward: GTAACACCAAGGAAGATGGGACC
	reverse: TCATGTCCGTCTGGCAGCTTGA
VILIP-1	forward: CCTGCTCAACTACTCATTAAG
	reverse: GGACATCTATTGCCACCTT
XBP-1	forward: CGCAGCACTCAGACTATG
	reverse: GGTCCAACCTTGTCCAGAAT

2.6 Validation of Candidate Proteins by Western Blot Analysis

Retinas were dissected and centrifuged at 4°C for 20 min. Protein samples were separated by sodium dodecyl-sulfate polyacrylamide gel electrophoresis and transferred to polyvinylidene difluoride filter membranes (Millipore). The membranes were then blocked with 5% nonfat dry milk in TBS-T at room temperature for 2.5 h. Primary antibodies for FABP7 (1:500, CST,13347, United States), Caveolin1(1:500, Abcam, ab32577, United States), S100A6 (1:500, CST,13162, United States), Galectin-1 (1:500, CST,12936, United States), Visinin-like protein-1 (1:500, CST,49468, United States), XBP-1 (1:500, CST, 40435, United States), and GAPDH (1:2,000, CST,5174, United States) were added to the membranes and incubated with gentle rocking at room temperature for 1.5 h. The corresponding secondary antibody was then added and incubated at room temperature for 1 h. Finally, protein visualization was performed using an enhanced chemiluminescence system (Millipore) and quantification was carried out with Image Lab 6.0 software (Bio-Rad).

2.7 Immunofluorescence of Retinal Cryosections

Eyes were prepared for cryosectioning by enucleation and embedding in optimal cutting temperature compound (Sakura Finetek, Torrance,CA) at -80degC. Sections of 5 μ m thickness were cut on a cryostat and placed on poly-L-lysine coated slides, followed by fixation in cold acetone on ice for 8 minutes. The sections were permeabilized using PBS with 0.05% Triton-X for 5 minutes at room temperature (RT) and then blocked with 5% BSA in PBS at RT for 1 hour. Primary antibodies were incubated overnight at 4°C in a humidity chamber, followed by incubation with secondary antibodies conjugated with a fluorescent dye (Alexa Fluor 488; Molecular Probes/Invitrogen) for 1 hour at RT. Nuclei were stained with 4',6'-diamidino-2-phenindole(DAPI) for 6 min at room temperature. Images were captured using a confocal microscope (LSM 980; Carl Zeiss Meditec, Oberkochen, Germany) with excitation filters for DAPI and green set at 450 nm and 549 nm respectively. The levels of staining were determined by calculating the percentage of area with positive fluorescence in the samples.

2.8 Cell culture and Oxygen and glucose deprivation/reoxygenation (OGDR) treatment

The human trabecular meshwork (TM) cells and human retinal endothelial cells (HRECs) were purchased from Procell Life Science & Technology Co., Ltd. (Wuhan, China), while the 661W photoreceptor cell line was obtained from the American Type Culture Collection (Manassas, VA, USA).

In brief, Cell cultures were maintained in complete TM cell medium (Procell, Wuhan, China), which contained 5% (v/v) heat-inactivated fetal bovine serum, 1% TM cell growth supplement. Human retinal endothelial cells (HRECs) were grown in endothelial cell medium (ECM, ScienCell, USA) especially containing 1% endothelial cell growth supplement. Mouse retinal 661W cells were cultured in Dulbecco's modified Eagle's medium (DMEM, Gibco, CA, USA) supplemented with 10% fetal bovine serum (FBS; Gibco, Carlsbad, CA, USA). The cells were maintained at 37 degC in a humidified 5% CO2 incubator. When cells grew to 80% ~ 90% fusion, the cells at logarithmic growth stage were used for the experiment.

To mimic the murine model of RIR in vitro, cells were subjected to oxygen and glucose deprivation for 3 h and subsequently returned to their normal environment (37 degC, normoxic) and normal medium (DMEM supplemented with 10% FBS and glucose [4.5 g/L]) for 24 h prior to harvest. The cells were transferred into serum and glucose-free medium and placed under hypoxic conditions (5% CO2 and 95% N2) in a 37 degC incubator for 3 h. Reperfusion was performed by exposing the cells to normoxic culture conditions and culturing them in DMEM supplemented with 10% FBS and glucose (4.5 g/L) in a 37 degC incubator for 24 h.

2.9 Cell immunofluorescence assay

The mouse TM, HRECs and 661W cells were subjected to oxygen and glucose deprivation for 3 h followed by 24 h of OGDR. After OGDR, the cells were fixed with 4% PFA for 30 min and washed several times with PBS. The primary antibodies targeted FABP7 (1: 200) and Caveolin1 (1:200). Cell nuclei were stained with DAPI. Fluorescence images were acquired by two independent observers with a Zeiss fluorescence microscope.

2.10 Statistical Analysis

The study data were presented as mean +- standard deviation (SD). Statistical analysis was conducted using SPSS 23.0 software (SPSS Inc., USA). Student's t-test was performed to compare the normally distributed variables between the two groups. Group differences were considered significant if $p < 0.05$. For functional enrichment analysis of GO and pathway analysis, Fisher's exact test (two-tailed) was used to examine the enrichment of differentially expressed proteins compared to all identified proteins, and a corrected p -value of < 0.05 was considered statistically significant. Proteins with a fold change greater than 1.5 and a p -value < 0.05 were considered differentially abundance proteins.

3. Results

3.1 Protein Abundance on Retinas in AOH Mice

The experimental workflow is depicted in Fig. 1, where MS-based proteomics was utilized to investigate the AOH retina proteome to identify molecules potentially involved in the pathogenic changes in retinal hypoxia-ischemia caused by acute glaucoma. Using a cutoff of 1.5-fold changes and a p value < 0.05 , 92 Differentially abundance proteins were identified in the AOH group compared to the control group. To visualize the distribution of proteins with differential expression, a volcano plot was generated (Fig. 2A). Out of the 92 differentially abundance proteins, 58 were significantly up-regulated while 34 were down-regulated in the AOH retina (Table 2). Notably, the expression levels of Cav-1, S100a6, FABP7, and Galectin-1 were up-regulated, while VILIP-1 and XBP-1 were among the downregulated proteins with a fold change greater than 1.5.

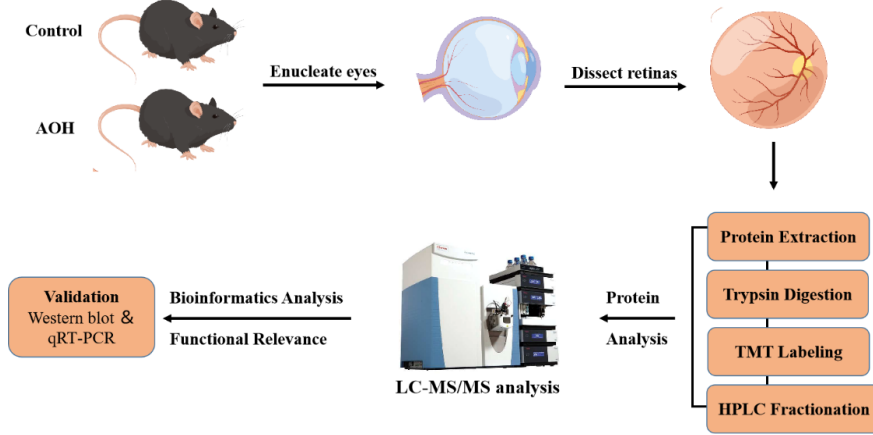


Figure 1 . Proteomics workflow schematic. Mass spectrometry-based proteomics of retinal samples collected from C57BL/6 adult mice (control: n = 3; AOH: n = 3).

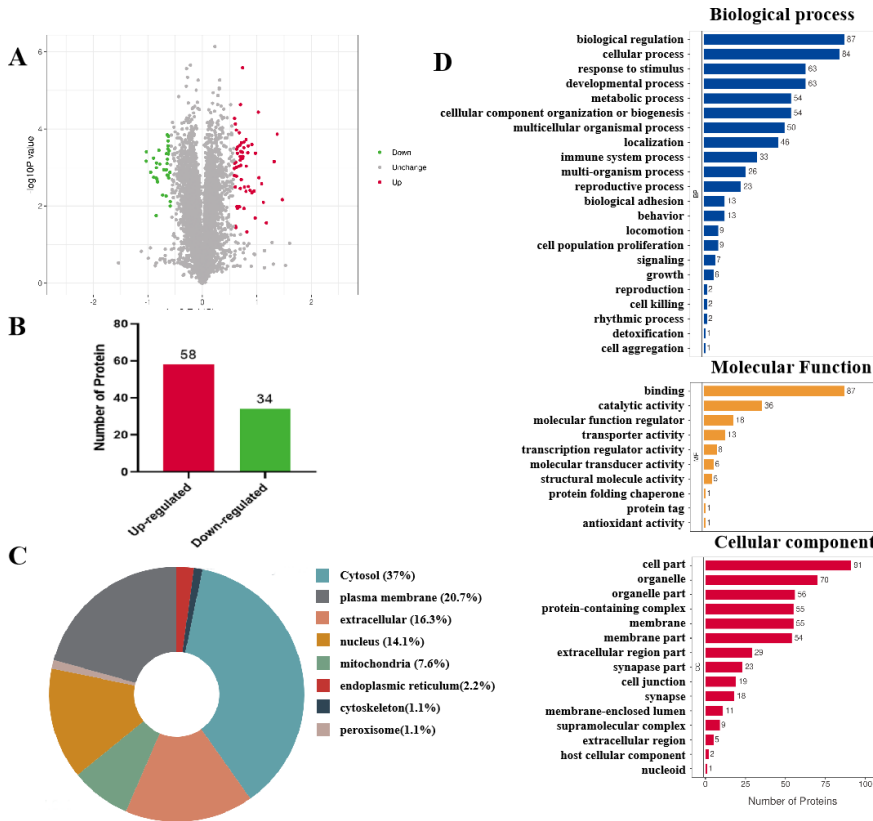


Figure 2. functional classification of the differentially expressed retinal proteins. (A) Volcano plot showing variations in protein abundances. x-axis, log₂; y-axis, -log of P-value. Green, downregulated proteins; red, upregulated proteins; grey, unchanged proteins. (B) Histogram representing the distribution of differentially expressed proteins. (C) The subcellular localization of altered proteins. (D) Categories of differentially expressed proteins according to Gene ontology (GO), including biological process, molecular function, and cellular component.

Table 2. List of differentially abundance proteins in AOH group compared with control group.

UniProt accession	Gene name	Protein description	AOH vs. Cha
P98086	C1qa	Complement C1q subcomponent subunit A	2.7657
Q3ULW8	Parp3	Protein mono-ADP-ribosyltransferase PARP3	2.5903
Q9CYL5	Glipr2	Golgi-associated plant pathogenesis-related protein 1	2.4901
Q91WP6	Serpina3n	Serine protease inhibitor A3N	2.2593
P14106	C1qb	Complement C1q subcomponent subunit B	2.1725
P49935	Ctsh	Pro-cathepsin H	2.1260
P50543	S100a10	Protein S100-A10	2.0532
Q9Z0E6	Gbp2	Guanylate-binding protein 2	2.0358
Q64282	Ifit1	Interferon-induced protein with tetratricopeptide repeats 1	1.9625
P20065	Tmsb4x	Thymosin beta-4	1.9551
Q06890	Clu	Clusterin	1.9322
Q9R118	Htra1	Serine protease HTRA1	1.8763
P03995	Gfap	Glial fibrillary acidic protein	1.8761
P13597	Icam1	Intercellular adhesion molecule 1	1.8351
O89017	Lgmn	Legumain	1.7948
Q64345	Ifit3	Interferon-induced protein with tetratricopeptide repeats 3	1.7940
P24452	Capg	Macrophage-capping protein	1.7847
Q61233	Lcp1	Plastin-2	1.7613
P14901	Hmox1	Heme oxygenase 1	1.7487
P15655	Fgf2	Fibroblast growth factor 2	1.7442
O70370	Ctss	Cathepsin S	1.7409
P28076	Psmb9	Proteasome subunit beta type-9	1.7077
P29533	Vcam1	Vascular cell adhesion protein 1	1.7005
Q9QZ03	Slc39a1	Zinc transporter ZIP1	1.6969
Q641K1	Agtpbp1	Cytosolic carboxypeptidase 1	1.6939
O35309	Nmi	N-myc-interactor	1.6711
O35955	Psmb10	Proteasome subunit beta type-10	1.6686
P15379	Cd44	CD44 antigen	1.6664
P14069	S100a6	Protein S100-A6	1.6624
Q64339	Isg15	Ubiquitin-like protein ISG15	1.6408
P51642	Cntf	Ciliary neurotrophic factor	1.6376
Q61263	Soat1	Sterol O-acyltransferase 1	1.6310
Q9WVA4	Tagln2	Transgelin-2	1.6300
P42227	Stat3	Signal transducer and activator of transcription 3	1.6238
O54983	Crym	Ketimine reductase mu-crystallin	1.6208
P10833	Rras	Ras-related protein R-Ras	1.6205
O70458	Osmr	Oncostatin-M-specific receptor subunit beta	1.6204
P26041	Msn	Moesin	1.6162
P21981	Tgm2	Protein-glutamine gamma-glutamyltransferase 2	1.6036
Q8R2Q8	Bst2	Bone marrow stromal antigen 2	1.5996
P08226	Apoe	Apolipoprotein E	1.5945
Q9QZU9	Ube2l6	Ubiquitin/ISG15-conjugating enzyme E2 L6	1.5680
Q9WUU7	Ctsz	Cathepsin Z	1.5625
Q6Q899	Ddx58	Antiviral innate immune response receptor RIG-I	1.5620
Q9WV32	Arpc1b	Actin-related protein 2/3 complex subunit 1B	1.5537
Q9EQK5	Mvp	Major vault protein	1.5457
P21958	Tap1	Antigen peptide transporter 1	1.5429

UniProt accession	Gene name	Protein description	AOH vs.
Q5U4C3	Scaf1	Splicing factor, arginine/serine-rich 19	1.5420
P29391	Ftl1	Ferritin light chain 1	1.5394
P08905	Lyz2	Lysozyme C-2	1.5333
P42225	Stat1	Signal transducer and activator of transcription 1	1.5315
Q00493	Cpe	Carboxypeptidase E	1.5253
P50427	Sts	Steryl-sulfatase	1.5240
Q91VJ2	Cavin3	Caveolae-associated protein 3	1.5205
P35918	Kdr	Vascular endothelial growth factor receptor 2	1.5076
P49817	Cav1	Caveolin-1	1.5060
Q61107	Gbp4	Guanylate-binding protein 4	1.5015
P16045	Lgals1	Galectin-1	1.5014
O35426	Xbp1	X-box-binding protein 1	0.7938
P62761	Vsnl1	Visinin-like protein 1	0.7011
Q61554	Fbn1	Fibrillin-1	0.6651
Q8BTI9	Pik3cb	Phosphatidylinositol 4,5-bisphosphate 3-kinase catalytic subunit beta isoform	0.6647
P14094	Atp1b1	Sodium/potassium-transporting ATPase subunit beta-1	0.6624
Q56A07	Scn2b	Sodium channel subunit beta-2	0.6553
P17879	Hspa1b	Heat shock 70 kDa protein 1B	0.6519
B2RSH2	Gnai1	Guanine nucleotide-binding protein G(i) subunit alpha-1	0.6503
Q9WVB0	Rbpms	RNA-binding protein with multiple splicing	0.6494
Q9JJZ8	Cnga3	Cyclic nucleotide-gated cation channel alpha-3	0.6484
Q80TL4	Phf24	PHD finger protein 24	0.6473
O55042	Snca	Alpha-synuclein	0.6459
Q6PHS9	Cacna2d2	Voltage-dependent calcium channel subunit alpha-2/delta-2	0.6441
Q7TQD2	Tppp	Tubulin polymerization-promoting protein	0.6416
P0C192	Lrrc4b	Leucine-rich repeat-containing protein 4B	0.6401
Q3V384	Afg1l	AFG1-like ATPase	0.6391
Q9WUC3	Ly6h	Lymphocyte antigen 6H	0.6386
P11798	Camk2a	Calcium/calmodulin-dependent protein kinase type II subunit alpha	0.6352
O35526	Stx1a	Syntaxin-1A	0.6332
Q3USH1	Insyn2a	Inhibitory synaptic factor 2A	0.6316
Q91VR8	Brk1	Protein BRICK1	0.6305
O55240	Rdh5	Retinol dehydrogenase 5	0.6113
Q9EP96	Slco1a4	Solute carrier organic anion transporter family member 1A4	0.6038
Q08331	Calb2	Calretinin	0.5821
P15409	Rho	Rhodopsin	0.5745
P63040	Cplx1	Complexin-1	0.5654
P15499	Prph2	Peripherin-2	0.5577
Q9ESG4	Cltn	Collectrin	0.5573
Q9CX11	Utp23	rRNA-processing protein UTP23 homolog	0.5561
Q5EBJ4	Ernm	Ermin	0.5536
Q8C838	Trarg1	Trafficking regulator of GLUT4 1	0.5380
Q9D387	Lamp5	Lysosome-associated membrane glycoprotein 5	0.5375
O35599	Opn1mw	Medium-wave-sensitive opsin 1	0.5180
P86046	Kcnj13	Inward rectifier potassium channel 13	0.4900
Q8BHB9	Clic6	Chloride intracellular channel protein 6	0.4892

2.2 GO Enrichment Analysis of Differentially Abundance

Proteins in AOH Mice

The differentially abundance proteins in this study were annotated using GO categories, including biological process, cellular component, and molecular function, as well as subcellular localization, to elucidate their properties and functions. The top four GO keywords in biological process were biological regulation, cellular process, response to stimulus, and developmental process, with 87, 84, 63, and 63 differentially abundance proteins, respectively. The cellular component analysis revealed that the DEPs were enriched in cell, organelle, and organelle part, with 91, 70, and 56 differentially abundance proteins, respectively. The most prevalent terms in molecular function were binding (87 proteins), catalytic activity (36 proteins), and molecular function regulator (18 proteins). Subcellular localization predictions showed that the greater percentages of differentially abundance proteins were enriched in the cytoplasm (37.0%), plasma membrane (20.7%), and extracellular (16.3%) (Fig. 2C). Based on GO functional classification, the differentially abundance proteins were categorized into 55 GO terms, including 25 biological process terms, 16 cellular component terms, and 14 molecular function terms. (Fig. 2D)

3.3 Functional Enrichment Analysis of Differentially Expressed Proteins in AOH Mice

The study employed KEGG analysis to identify biological pathways for the differentially abundance proteins between the two groups. The top 20 highly enriched pathways were displayed in Fig. 3A and 3B, including the JAK-STAT signaling pathway, neuroactive ligand-receptor interaction, GABAergic synapse, phototransduction, glutamatergic synapse, and cell adhesion molecules. Domain enrichment analysis revealed that the differentially abundance proteins were mainly linked to Guanylate-binding protein, C-terminal domain superfamily, Visual pigments (opsins) retinal binding site, Opsin, Guanylate-binding protein/Atlastin, and C-terminal, Intercellular adhesion molecule/vascular cell adhesion molecule, N-terminal (Fig. 3C). Furthermore, the study used the STRING program to identify the PPI networks for both the up- and down-regulated genes, and the results suggested a close relationship among GFAP, FABP7, Calb2, Snca, Fgf2, and Caveolin1 (Figure 3D).

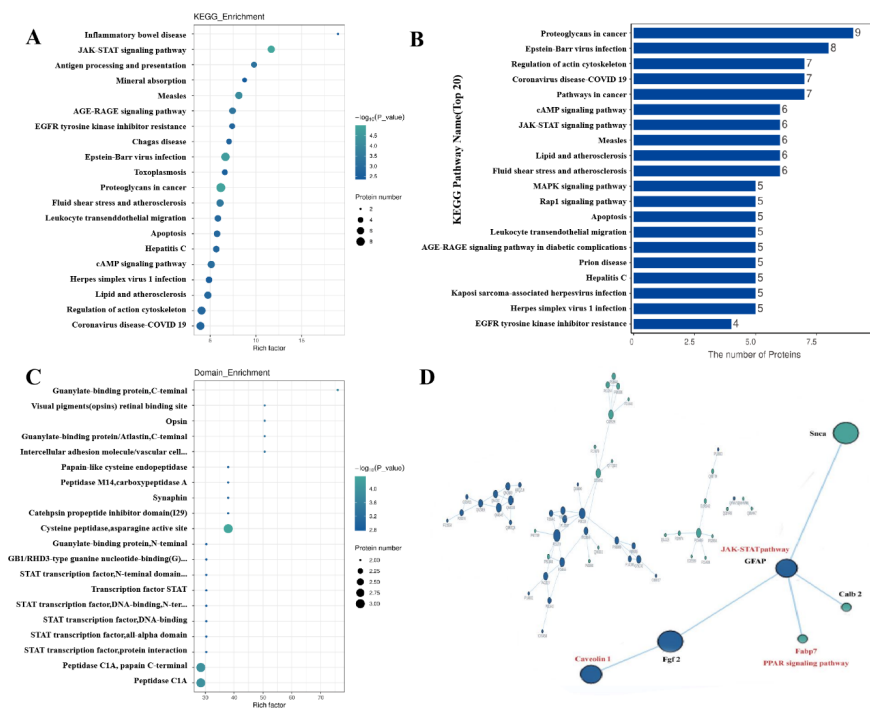


Figure 3. KEGG pathway enrichment analysis of differentially expressed proteins. **A** Bubble diagram representing the enrichment analysis of differentially expressed proteins in KEGG pathways. **B** Pathways analysis of significantly changed proteins. The top 20 signaling pathways were determined by using the

KOALA(KEGG Orthology And Links Annotation)soft well. **C** Bubble diagram of differentially abundant proteins enriched by Protein Domain. **D** In total 51 proteins formed a protein-protein-interacting (PPI) network and PPI network between 6 key targets.

2.4 Validation of Candidate Proteins

The study focused on investigating the JAK-STAT signaling pathway and PPAR signaling pathway as both are involved in neuronal survival, inflammation, proliferation, and vascular morphology and function. Several proteins associated with these pathways, including Caveolin1, FABP7, S100a6, Galectin-1, VILIP, and xbp-1, were selected for validation using quantitative real-time PCR (qRT-PCR) and western blotting. The results showed that Caveolin1, FABP7, S100a6, and Galectin-1 were significantly up-regulated in AOH retinal tissue compared to the sham group, while VILIP and xbp-1 were down-regulated (Fig. 4A). The western blotting results were consistent with the qRT-PCR results (Fig. 4B-G).

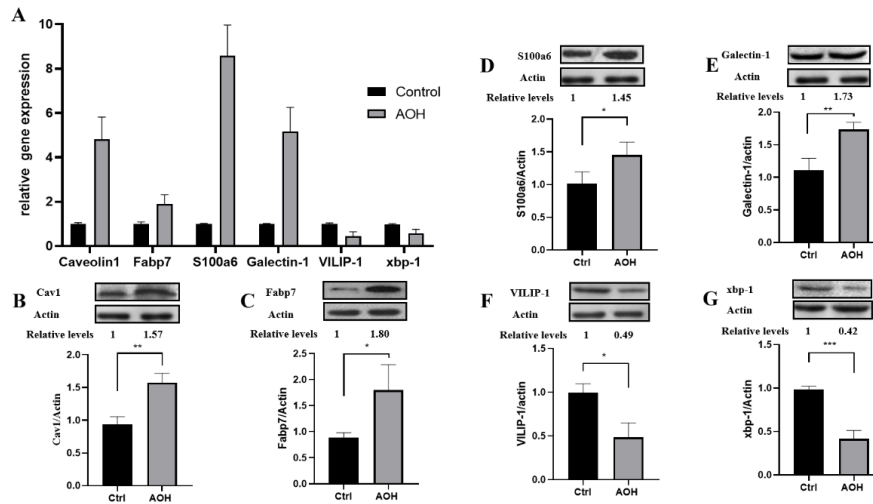


Figure 4. Verification of differentially abundant proteins. **(A)** Quantitative analysis of Caveolin1, FABP7, S100a6, Galectin-1, VILIP and xbp-1 mRNA level. **(B-H)** Representative western blot images and quantification of Caveolin1, FABP7, S100a6, Galectin-1, VILIP and xbp-1. All tests were analyzed by a *t*-test with two-tailed and all data were expressed as the mean \pm SEM ($n = 3$ each group). * $p < 0.05$, ** $p < 0.01$, *** $p < 0.001$.

Immunofluorescence staining of retinal sections was used to show the expression and location of FABP7 and Cav-1 after AOH. FABP7 was found to be present in the inner retinal layer and showed increased intensity after AOH. Anti-Cav-1 staining showed increased immunoreactivity of Cav-1 located in the retinal endothelium (Fig. 5A-B). Our research has demonstrated that the expression of Cav-1 progressively increases in trabecular meshwork cells and human retinal endothelial cells during the development of retinal hypoxia/ischemia injury. Furthermore, exposure of photoreceptor cells to OGDRO resulted in a significant upregulation of FABP7(Fig. 5C-D).

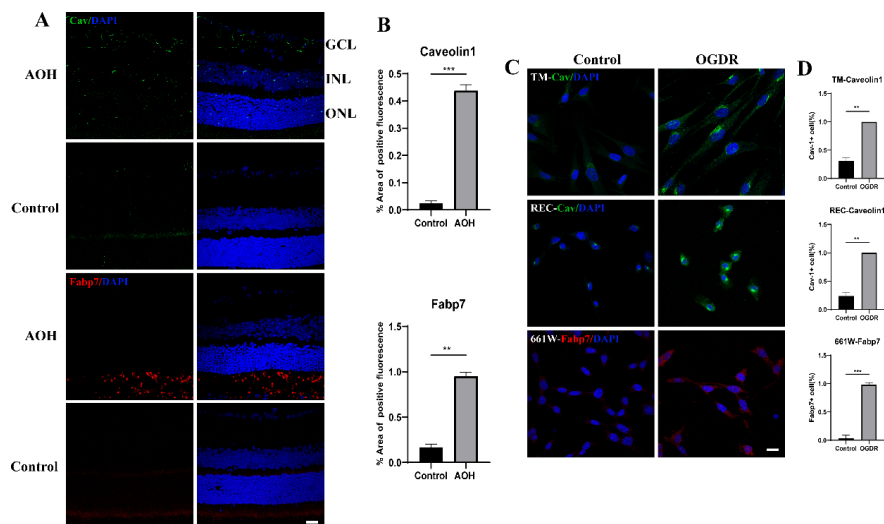


Figure 5. Protein immunofluorescence analyses of retinal sections. **(A)** Representative images of Caveolin-1 and FABP7 staining in retinal sections of AOH and control group. Blue indicated the DAPI staining whereas green indicated the Caveolin1 staining. Scale bar: 20 μ m (n = 3). **(B)** The quantification of the percentage of area with positive green fluorescence for samples shown in. **(C)** Representative images of immunofluorescence staining targeting Caveolin-1 in TM, REC cells and FABP7 in 661W cell line exposed to OGDR. Scale bar: 20 μ m (n = 3). **(D)** Analysis of quantification of percentage of staining positive cells with Cav-1 (green) and FABP7 (red).

3. Discussion

The present study utilized an unbiased proteomics approach to investigate the molecular mechanisms underlying glaucomatous neurodegeneration in an experimental glaucoma model induced by AOH. Experimentally induced retinal I/R injury is an established model of glaucoma injury that ultimately leads to RGC apoptosis[14]. Proteomics, which is centered around the analysis of proteins, plays a crucial role in enhancing our understanding of pathophysiological pathways in glaucoma. By examining protein abundant, modifications, and interactions, proteomics can provide a comprehensive link between genotypic and phenotypic changes. Furthermore, since many therapies target proteins, proteomics can contribute to drug development as well as providing insights into cellular signaling and function. Glaucoma researchers have long been studying protein expression, modifications, and interactions in experimental models and postmortem human tissues with glaucoma[5,6,9]. TMT proteomics, a novel method of protein mass spectrometry, has emerged as a powerful tool for screening differentially expressed proteins in various fields, including tumor metastasis[15], autoimmune disease[16] and HIV infection[17]. This study is the first to use TMT quantitative proteomics technology combined with 2D LC-MS/MS to screen for differentially expressed proteins in the AOH-induced glaucoma model.

Table 2 presents a comprehensive list of significantly altered proteins, including their fold changes and corresponding p-values. To validate the results, Caveolin1, FABP7, S100a6, Galectin-1, VILIP, and xbp-1 proteins, known for their association with neurodegeneration, neuroinflammation, and lipogenesis, were selected for further investigation. The western blotting and real-time PCR results confirmed the proteomics findings. The S100 protein family plays a significant role in various diseases such as cancer, metabolic disease, neurological disease, and vascular calcification. S100 proteins may facilitate cell signal transduction in response to internal or external stimuli. S100a6, a member of the S100 protein family, has been implicated in the inflammatory response to ischemic conditions[18]. A study by Stepanov et al. found that the pro-inflammatory S100a6 levels are directly proportional to the severity of retinal ischemia[19]. The findings from our study provide valuable insights into the mechanisms underlying retinal ischemia and the related

inflammatory response. Our data suggest that the increase in S100a6 levels in the AOH retinal under ischemic conditions could be indicative of inflammation being a major factor in the development of this condition. The LGALS1 gene encodes galectin-1, a member of the galactoside-binding lectin family that is crucial for angiogenesis. The statement of retinal ischemia causes the release of a variety of inflammatory and angiogenic cytokines, which in consequence encouraged galectin-1 up-expression[20]. Interestingly, galectin-1 has been found to enhance cerebral ischemia recovery by targeting vascular remodeling, which highlights its potential as a therapeutic target for retinal ischemia[21]. Galectin-1 has also been shown to aid cerebral ischemia recovery by focusing on vascular remodeling.

Another protein that we investigated was VILIP-1, a member of the neuronal calcium sensor family that regulates various neuronal functions, including ion channel regulation, learning, and neuronal growth. However, in the pathogenesis of stroke, VILIP-1 acts as a neurotoxic factor for neurons when transient ischemia disturbs calcium homeostasis[22]. These results have important implications for developing strategies to prevent neuronal damage during ischemia. Furthermore, our study also highlighted the critical role of X box binding protein 1 (XBP 1), a key transcription regulator of the unfolded protein response, in mediating adaptation to endoplasmic reticulum stress [23]. Based on our findings, we hypothesize that a feedback loop may exist between XBP 1, ERS, and lipogenesis, which could provide novel insights into the mechanisms underlying the development of retinal ischemia.

The STRING data analysis provided valuable insights into the potential functions of FABP7 and Caveolin1 in the PPAR/JAK-STAT signaling pathway, as they were found to be in the center of the proteomics function network (fig.3D). An intriguing recent study suggests that FABP7 may have an impact on Cav-1 expression, thereby regulating lipid raft function in astrocytes, which could have important implications for the pathogenesis of neurodegenerative disorders[24]. FABPs are small cytosolic nonenzymatic proteins (14-15 kDa) that bind to long-chain fatty acids and play critical roles in cellular uptake and transport of fatty acids, intracellular signal transduction, and regulation of gene expression[25]. After cerebral ischemia, FABP7 expression is upregulated in neural stem/progenitor cells[26], and our findings indicate that FABP7 is also significantly upregulated in the retina during the pathogenesis of retinal ischemia. Immunofluorescence data revealed that FABP7 is primarily expressed in the photoreceptor layer of the retina, where the most prevalent polyunsaturated fatty acids (PUFAs) are found in photoreceptor membrane phospholipids. Interestingly, FABP7 has been demonstrated to bind to docosahexaenoic acid (DHA) *in vitro*, which is one of the most abundant PUFAs in the retina and critical for retinal function[27]. Furthermore, in FABP7-knockout mice, there were notable changes in retinal morphology, including increased acellular strands, less branching of the microvasculature, and endothelial cell loss, which are characteristic of early diabetic retinopathy[28]. Taken together, our findings suggest that FABP7 may play a crucial role in regulating photoreceptor function under 'stress' conditions, such as retinal ischemia, by modulating fatty acid uptake and transport and influencing lipid raft function.

The scaffolding protein Caveolin-1, which has been discovered to be increased in the AOH group, interacts with numerous signaling molecules. The ability of Caveolin-1 to interact with numerous signaling molecules and its presence in a variety of ocular cells, such as retinal vascular cells, Müller glia, retinal pigment epithelium, and typical aqueous humor outflow cells, highlights its importance in transcellular transport, endocytosis, cell proliferation, membrane lipid homeostasis, and signal transduction. As a critical regulator of caveolae and their molecular components, Caveolin-1 is essential for maintaining the integrity of the blood-retinal barrier, regulating ocular inflammatory signaling, preventing pathogen entry at the ocular surface, and facilitating aqueous humor drainage. Moreover, the importance of Cav-1's cell-specific inflammatory regulatory characteristics is exemplified in numerous studies of acute lung injury, where its deficiency has been shown to reduce local cytokine production [29]. In the retina, retina-specific Cav-1 deficiency has been demonstrated to suppress STAT3 phosphorylation after retinal damage, highlighting the protein's role in retinal neuroprotection[30]. The observed increase in Cav-1 expression in the AOH model retina suggests that it may act as a protective factor for retinal neuroprotection, underscoring its importance in maintaining the delicate balance of ocular homeostasis.

In response to acute IOP elevation, the retina undergoes significant changes in several key processes, including cellular and developmental processes, as well as its response to stimulus. Our KEGG pathway enrichment analysis identified several pathways that were primarily involved in the JAK-STAT signaling pathway, neuroactive ligand-receptor interaction, GABAergic synapse, and phototransduction. By using a combination of functional pathways and protein-protein interaction analysis tools, we were able to identify specific pathways that are impacted by high IOP. Interestingly, our analysis revealed a close relationship among GFAP, FABP7, and Caveolin1, which are all associated with the JAK-STAT and PPAR signaling pathways that were upregulated or induced in the animal model of high IOP (fig.6). These findings suggest that there may be complex interactions between these proteins that play a crucial role in the retinal response to elevated IOP. Further studies on these pathways and proteins may shed light on potential targets for therapeutic interventions to prevent or treat ocular diseases associated with high IOP.

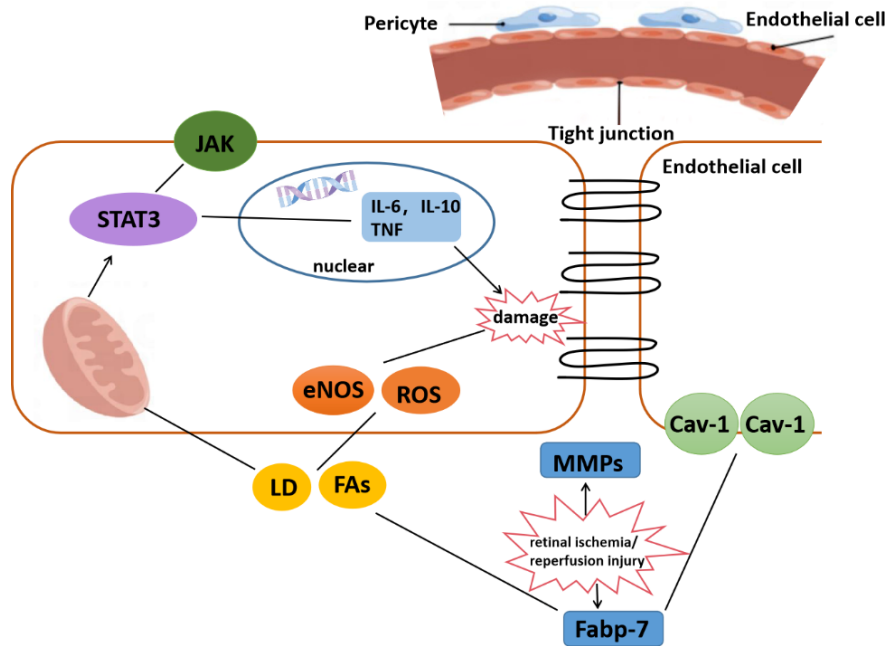


Figure 6. Diagram illustrating the pathway by which FABP7 and Caveolin1 are involved in the biological functions of neuroinflammation and retinal lipid homeostasis, contributing to the pathogenesis of acute glaucoma. Fabp-7, Fatty acid-binding protein 7; MMPs, matrix metalloproteinases; Cav-1, caveolin-1; LD, lipid droplet; FAs, fatty acids; ROS, Reactive Oxygen Species; eNOS, Nitric oxide synthase; STAT3, signal transducer and activator of transcription 3; JAK, janus kinase; IL-6, Interleukin-6; IL-10, Interleukin-10; TNF, tumour necrosis factor.

The JAK/STAT signaling pathway is a fascinating and multifaceted intracellular signal transduction pathway that plays a crucial role in many biological processes, including hematopoiesis, immune fitness, tissue repair, inflammation, apoptosis, and adipogenesis[31]. Besides, PPAR family of nuclear receptors plays a major regulatory role in energy homeostasis and metabolic function. Research conducted by Sun X et al. has shown that the activation of PPAR signal transduction in macrophages can lead to the downregulation of JAK-STAT signals and the enhancement of fatty acid metabolism[32]. Cholesterol homeostasis is crucial for neuronal survival[33]. Retinal lipid homeostasis is also tightly regulated by several mechanisms implicated in retinal lipid trafficking between neurons and glial cells and eliminating lipids through blood circulation[34]. A drop in cholesterol level in the cell's membrane causes dissociation and dysfunction of glutamate transporter lipid rafts. The excess glutamate level at the synaptic level leads to neurotoxicity. We can assume that modulations of cell membrane proteins in lipid rafts are possible in glaucomatous neuropathy. JAK-STAT

signals and PPAR also exhibit marked anti-inflammatory capacities[35], which can play a role in protecting the neurons from neuroinflammation and subsequent neuronal loss, an essential pathophysiological process in glaucomatous neurodegeneration. Moreover, PPRA-mediated STAT3 downregulation has been shown to interfere with STAT-dependent transcriptional activity, which may also contribute to the anti-inflammatory action of PPAR activation[36]. Neuroinflammation leading to neuronal loss is also an important pathophysiological process of glaucomatous neurodegeneration.

Using a multi-step data analysis procedure, the researchers were able to identify and quantify the relative abundances of proteins and compare them between experimental groups. This approach allowed for a thorough evaluation of potential differences in protein expression and provided a statistically sound framework for interpretation of the data. Furthermore, the reliance on current protein databases and previously published data from a wide range of biological systems highlights the interdisciplinary nature of modern scientific research. By pooling information from various sources, researchers were able to identify potential protein-protein interactions and pathways that may be relevant to the observed findings. It is important to note that the results presented in this study are based on interpretations of the data and predicted pathways. However, these findings represent an important step forward in understanding the mechanisms underlying conditions such as acute glaucoma and elevations in intraocular pressure. As with any scientific study, further investigation is necessary to confirm and expand upon these findings, but the potential implications for future research and treatment are promising.

5. Conclusions

In conclusion, we discovered many protein candidates that may be related to retinal ischemic injury in acute glaucoma using quantitative proteomics to analyze protein modifications in AOH retinas. For patients with acute glaucoma, the neuroinflammation and retinal lipid homeostasis may be involved and represent potential therapeutic approaches. The upregulation of FABP7 and Cav-1 levels in ischemia retinas highlights the intricate network of signaling pathways involved in retinal dysfunction. While our study provides a foundation for understanding the pathogenesis of retinal ischemia, further research is needed to fully elucidate the underlying mechanisms and identify novel therapeutic interventions to treat acute glaucoma.

Author Contributions: G.H.: Data curation; formal analysis; investigation. Y.L.: Methodology; investigation; project administration. F.T.: Investigation; methodology; data curation. H.H.: Investigation; resources. Q.C.: Validation; data curation. N.S.: Investigation; resources; project administration. L.C.: Supervision; project administration. F.X.: Project administration; funding acquisition. C.S.: Conceptualization; funding acquisition; writing—review and editing; writing—original draft. All authors have read and agreed to the published version of the manuscript.

Funding: This work was supported by Guangxi Natural Science Foundation Program (Grant No. 2020GXNSFB159057), Guangxi Clinical Ophthalmic Research Center (No. Guike AD19245193), and the National Natural Science Foundation (No. 82000925, 82070982,82060179).

Declaration of Competing Interest: The authors declare no competing financial interest.

Reference

- [1] Tham YC, Li X, Wong TY, Quigley HA, Aung T, Cheng CY. Global prevalence of glaucoma and projections of glaucoma burden through 2040: a systematic review and meta-analysis. *Ophthalmology*.2014;121(11):2081-2090.
- [2] Khazaeni B, Khazaeni L. Acute Closed Angle Glaucoma. In: Treasure Island (FL): Copyright © 2022, StatPearls Publishing LLC.; 2022:pp5-35.
- [3] Chang EE, Goldberg JL. Glaucoma 2.0: neuroprotection, neuroregeneration, neuroenhancement. *Ophthalmology*.2012;119(5):979-986.
- [4] Pascale A, Drago F, Govoni S. Protecting the retinal neurons from glaucoma: lowering ocular pressure is not enough. *Pharmacol Res*. 2012;66(1):19-32.

- [5] Mirzaei M, Gupta VK, Chitranshi N, et al. Retinal proteomics of experimental glaucoma model reveal intraocular pressure-induced mediators of neurodegenerative changes. *J Cell Biochem.* 2020;DOI: 10.1002/jcb.29822.
- [6] Reinehr S, Guntermann A, Theile J, et al. Proteomic Analysis of Retinal Tissue in an S100B Autoimmune Glaucoma Model. *Biology (Basel).* 2021;11(1):16.
- [7] Liu X, Liu X, Wang Y, et al. Proteome Characterization of Glaucoma Aqueous Humor. *Mol Cell Proteomics.* 2021;20:100117.
- [8] Nättinen J, Aapola U, Nukareddy P, Uusitalo H. Clinical Tear Fluid Proteomics-A Novel Tool in Glaucoma Research. *Int J Mol Sci.* 2022;23(15):8136.
- [9] Yang X, Hondur G, Li M, et al. Proteomics Analysis of Molecular Risk Factors in the Ocular Hypertensive Human Retina. *Investigative ophthalmology & visual science.* 2015;56(10):5816-5830.
- [10] Huang Y, Li Z, van Rooijen N, Wang N, Pang CP, Cui Q. Different responses of macrophages in retinal ganglion cell survival after acute ocular hypertension in rats with different autoimmune backgrounds. *Experimental eye research.* 2007;85(5):659-666.
- [11] Chi W, Li F, Chen H, et al. Caspase-8 promotes NLRP1/NLRP3 inflammasome activation and IL-1 β production in acute glaucoma. *Proc Natl Acad Sci U S A.* 2014;111(30):11181-11186.
- [12] Ye D, Xu Y, Shi Y, et al. Anti-PANoptosis is involved in neuroprotective effects of melatonin in acute ocular hypertension model. *J Pineal Res.* 2022;73(4):e12828.
- [13] Pang IH, Clark AF. Inducible rodent models of glaucoma. *Prog Retin Eye Res.* 2020;75:100799.
- [14] Della Santina L, Inman DM, Lupien CB, Horner PJ, Wong RO. Differential progression of structural and functional alterations in distinct retinal ganglion cell types in a mouse model of glaucoma. *J Neurosci.* 2013;33(44):17444-17457.
- [15] Cao J, Wang Y, Dong R, et al. Hypoxia-Induced WSB1 Promotes the Metastatic Potential of Osteosarcoma Cells. *Cancer Res.* 2015;75(22):4839-4851.
- [16] Aqrabi LA, Galtung HK, Vestad B, et al. Identification of potential saliva and tear biomarkers in primary Sjögren's syndrome, utilising the extraction of extracellular vesicles and proteomics analysis. *Arthritis Res Ther.* 2017;19(1):14.
- [17] Burgener A, Rahman S, Ahmad R, et al. Comprehensive proteomic study identifies serpin and cystatin antiproteases as novel correlates of HIV-1 resistance in the cervicovaginal mucosa of female sex workers. *J Proteome Res.* 2011;10(11):5139-5149.
- [18] Mofid A, Newman NS, Lee PJ, et al. Cardiac Overexpression of S100A6 Attenuates Cardiomyocyte Apoptosis and Reduces Infarct Size After Myocardial Ischemia-Reperfusion. *J Am Heart Assoc.* 2017;6(2):e004738.
- [19] Stepanov A, Usharova SA, Malsagova KA, et al. Tear Proteome Revealed Association of S100A Family Proteins and Mesothelin with Thrombosis in Elderly Patients with Retinal Vein Occlusion. *Int J Mol Sci.* 2022;23(23):14653.
- [20] Yamamoto T, Kanda A, Kase S, Ishida S. Hypoxia Induces Galectin-1 Expression Via Autoinduction of Placental Growth Factor in Retinal Pigment Epithelium Cells. *Investigative ophthalmology & visual science.* 2021;62(2):22.
- [21] Cheng YH, Jiang YF, Qin C, et al. Galectin-1 Contributes to Vascular Remodeling and Blood Flow Recovery After Cerebral Ischemia in Mice. *Transl Stroke Res.* 2022;13(1):160-170.
- [22] Laterza OF, Modur VR, Crimmins DL, et al. Identification of novel brain biomarkers. *Clin Chem.* 2006;52(9):1713-1721.

- [23] Ron D, Walter P. Signal integration in the endoplasmic reticulum unfolded protein response. *Nat Rev Mol Cell Biol.*2007;8(7):519-529.
- [24] Kagawa Y, Yasumoto Y, Sharifi K, et al. Fatty acid-binding protein 7 regulates function of caveolae in astrocytes through expression of caveolin-1. *Glia.* 2015;63(5):780-794.
- [25] Owada Y. Fatty acid binding protein: localization and functional significance in the brain. *Tohoku J Exp Med.*2008;214(3):213-220.
- [26] Kato T, Yoshioka H, Owada Y, Kinouchi H. Roles of fatty acid binding protein 7 in ischemic neuronal injury and ischemia-induced neurogenesis after transient forebrain ischemia. *Brain Res.*2020;1736:146795.
- [27] Anderson RE, Risk M. Lipids of ocular tissues. IX. The phospholipids of frog photoreceptor membranes. *Vision Res.*1974;14(1):129-131.
- [28] Su X, Tan QS, Parikh BH, et al. Characterization of Fatty Acid Binding Protein 7 (FABP7) in the Murine Retina. *Investigative ophthalmology & visual science.* 2016;57(7):3397-3408.
- [29] Jin Y, Lee SJ, Minshall RD, Choi AM. Caveolin-1: a critical regulator of lung injury. *Am J Physiol Lung Cell Mol Physiol.*2011;300(2):L151-160.
- [30] Reagan A, Gu X, Hauck SM, et al. Retinal Caveolin-1 Modulates Neuroprotective Signaling. *Adv Exp Med Biol.* 2016;854:411-418.
- [31] Owen KL, Brockwell NK, Parker BS. JAK-STAT Signaling: A Double-Edged Sword of Immune Regulation and Cancer Progression. *Cancers (Basel).* 2019;11(12):2002.
- [32] Sun X, Gao Y, Li Z, He J, Wu Y. Magnetic responsive hydroxyapatite scaffold modulated macrophage polarization through PPAR/JAK-STAT signaling and enhanced fatty acid metabolism. *Biomaterials.* 2023;295:122051.
- [33] Bretillon L, Thuret G, Grégoire S, et al. Lipid and fatty acid profile of the retina, retinal pigment epithelium/choroid, and the lacrimal gland, and associations with adipose tissue fatty acids in human subjects. *Experimental eye research.* 2008;87(6):521-528.
- [34] Fliesler SJ, Bretillon L. The ins and outs of cholesterol in the vertebrate retina. *J Lipid Res.* 2010;51(12):3399-3413.
- [35] Meeks KAC, Bentley AR, Adeyemo AA, Rotimi CN. Evolutionary forces in diabetes and hypertension pathogenesis in Africans. *Hum Mol Genet.* 2021;30(R1):R110-r118.
- [36] van der Meer DL, Degenhardt T, Väisänen S, et al. Profiling of promoter occupancy by PPARalpha in human hepatoma cells via ChIP-chip analysis. *Nucleic Acids Res.* 2010;38(9):2839-2850.

